Numerical Simulations for the Performance Optimization of $SnO_2/Cs_2AgInBr_6/CuO$ Lead-Free Perovskite Solar Cells

Leila Bechane
Laboratory of Materials Physics and its Applications, Faculty of Technology, University of M'sila, University Pole, Road Bourdj Bou Arreiridj, M'sila 28000, Algeria
leila.bechane@univ-msila.dz (corresponding author)

Hani Benguesmia
Electrical Engineering Laboratory (LGE), University of M'sila, University Pole, Road Bourdj Bou Arreiridj, M'sila 28000, Algeria
hani.benguesmia@univ-msila.dz

Hadda Tiouiri
Laboratory of Materials Physics and its Applications, Faculty of Technology, University of M'sila, University Pole, Road Bourdj Bou Arreiridj, M'sila 28000, Algeria
hadda.tiouiri@univ-msila.dz

Received: 11 May 2025 | Revised: 4 July 2025, 20 July 2025, and 1 September 2025 | Accepted: 6 September 2025

 DOI: https://doi.org/10.48084/etasr.12051

ABSTRACT

This study presents a numerical investigation of the photovoltaic performance of a lead-free double Perovskite Solar Cell (PSC) based on $Cs_2AgInBr_6$ as the absorber layer. Using the one-dimensional solar cell simulation tool AMPS-1D, critical device parameters, including active layer thickness and acceptor doping density, were evaluated. The impact of these parameters was tested on performance indicators, such as current density-voltage (J-V) characteristics, Open-Circuit Voltage (OVC), short-circuit current density (J_{SC}), fill factor (FF), and Power Conversion Efficiency (PCE). The results revealed that an optimal active layer thickness of 500 nm, combined with an acceptor density in the range of 10^{13}-10^{15} cm^{-3}, maximized the device performance. Under these conditions, the solar cell achieved a PCE of 24.96%, with J_{SC} = 29.40 mA/cm^2, V_{OC} = 0.969 V, and FF = 87.6%. These values underscored the promising potential of $Cs_2AgInBr_6$ as a non-toxic, eco-friendly alternative to lead-based perovskites in photovoltaic applications.

Keywords-AMPS-1D; $Cs_2AgInBr_6$ solar cells; heterojunction; SnO_2; CuO; efficiency

I. INTRODUCTION

The global energy crisis and the need for sustainability have increased the development of renewable energy sources [1]. Solar energy, which converts sunlight into electricity through photovoltaic systems, is a solution to the aforementioned challenges [2]. While solar panels can be applied across different environments (from deserts to urban rooftops), challenges remain regarding their efficiency, cost, and environmental impact.

Perovskite Solar Cells (PSCs) have gained significant attention due to their enhanced optoelectronic properties, including high absorption coefficients, tunable band gaps, and long charge carrier diffusion lengths [3-7]. These features have enabled PSCs to achieve high Power Conversion Efficiencies (PCEs) of 25% [8]. Despite these advancements, the instability under environmental stressors and the toxicity of lead (Pb) have led to the constraint of PSCs [9, 10]. To address these limitations, researchers turned their attention to lead-free alternatives, such as double perovskites with the general formula $A_2B^+B^{3+}X_6$, where A is a monovalent cation, B^+ and B^{3+} are mixed-valence metals, and X is a halide anion [11]. $Cs_2AgInBr_6$ is among the lead-free halide perovskites of interest, due to its direct band gap, excellent optical absorption, and intrinsic stability [12-14]. It has been demonstrated that solar cells based on $Cs_2AgInBr_6$ have achieved efficiencies up to 28%, compared to the lead-based panels [15, 16]. However, the optimization of device performance requires a deep understanding of the material's electronic properties and the influence of structural parameters, such as active layer thickness and doping concentrations. Copper oxide (CuO), a *p*-type semiconductor, has been widely used as a Hole Transport Layer (HTL) in photovoltaic devices due to its non-toxicity,

chemical stability, and favorable band alignment with perovskite absorbers [4, 16, 17]. Its high optical absorption coefficient (~105 cm^{-1}) and tunable band gap (1.2-2.1 eV) make it an ideal component for $Cs_2AgInBr_6$ in heterojunction solar cells [19-21]. Similarly, tin dioxide (SnO_2), an *n*-type transparent conducting oxide, can be used as an Electron Transport Layer (ETL) with high electron mobility and interfacial properties.

This study investigates the simulation of a double PSC composed of $Cs_2AgInBr_6$ using the AMPS-1D code. The primary objective is to evaluate how the variations in the active layer's thickness and acceptor density impact crucial parameters of the solar cell, including the performance parameters (*Jsc*, efficiency, FF, OCV) and the current-voltage characteristics (J-V).

II. SIMULATION

The proposed solar cell structure is illustrated in Figure 1, including a metal back contact, a 200 nm *p*-type CuO window layer, a *p*-type $Cs_2AgInBr_6$ absorber (thickness from 100 to 1000 nm), a 100 nm *n*-type SnO_2, and a transparent conducting oxide front contact. The structure was exposed to AM1.5 G light with an intensity of 100 mW/cm², at a temperature of 300 K. The material parameters used in these simulations were selected from [13-18]. Table I summarizes these parameters and their corresponding values for the CuO, perovskite (absorber layer), and SnO_2 components.

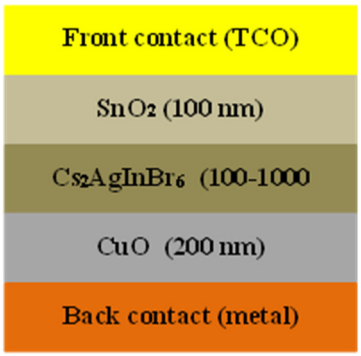

Fig. 1. Scehmatic representation of the simulated solar cell structure.

TABLE I. ADJUSTMENTS FOR THE SNO_2, $CS_2AGINBR_6$, AND CUO LAYERS USED IN THE SIMULATION

Parameter	*n*-SnO_2	*p*-$Cs_2AgInBr_6$	*p*-CuO
Thickness (nm)	100	100-1000	200
Dielectric constant	9	4.37	18.1
Electron mobility ($cm^2 V^{-1} s^{-1}$)	100	89.4	100
Hole mobility ($cm^2 V^{-1} s^{-1}$)	25	3.3	10^{-1}
Effective conduction band density (cm^{-3})	$2.2 \cdot 10^{18}$	$1.2 \cdot 10^{18}$	$2.2 \cdot 10^{19}$
Effective valence band density(cm^{-3})	$1.8 \cdot 10^{19}$	$1.73 \cdot 10^{18}$	$5.5 \cdot 10^{20}$
Acceptor concentration (cm^{-3})	0	10^{15}	10^{15}
Donor concentration (cm^{-3})	10^{16}	0	0
Band gap (eV)	3.6	1.57	1.4
Electron affinity (eV)	4.0	4.1	4.07
Gaussian defect density (cm^{-3})	10^{15}	10^{14}	10^{12}
Velocity SNL (cm/s)	10^7	10^7	10^7
Velocity SPL (cm/s)	10^7	10^7	10^7

III. RESULTS AND DISCUSSION

A. *Effect of $Cs_2AgInBr_6$ Active Layer Thickness*

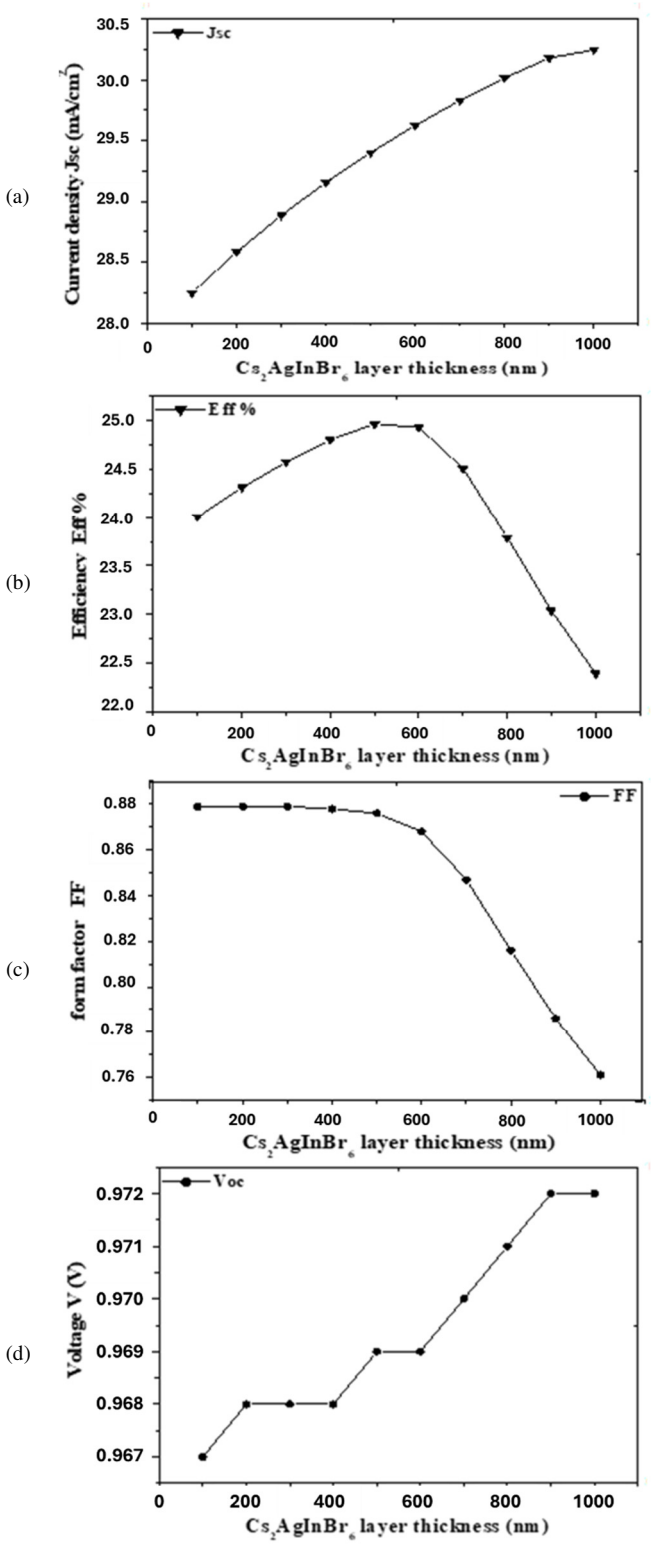

Fig. 2. The impact of Cs2AgInBr6 layer thickness on cell characteristic parameters (*Jsc*, PCE, FF, *Voc*).

Figure 2 presents the simulated output parameters of the $Cs_2AgInBr_6$ double PSC as a function of the absorber thickness. As shown in Figure 2(a), the short circuit current density (*Jsc*) increased with thickness. This trend is due to the increase in photon absorption within thicker layers which produce a higher photo-generated current. The PCE, as presented in Figure 2(b), rose with thickness until it reached its peak value at approximately 24.96% for a thickness of about 500 nm. After this point, the PCE dropped rapidly as the thickness further increased. The PCE maximum was a result of an optimum balance of two competing variables, those being photon absorption, which drove efficiencies at thinner layers, and carrier transport properties, limiting the efficiencies at thicker absorber layers. The FF variation with the absorber thickness is illustrated in Figure 2(c). As the thickness increased from 100 to 1000 nm, the FF decreased from 87.9% to 76.1%. This reduction was attributed to the higher series resistance and recombination occurring in thicker layers. In Figure 2(d), the OCV increased with thickness. This is likely due to the larger light absorption, increased charge accumulation, and a better electric field arrangement in the junction.

B. *Properties of Voltage Current*

Figure 3 displays the simulated current density-voltage (J-V) characteristics of the solar cell. These were modeled using the AMPS-1D software with the layer properties and Gaussian defect distributions defined in Table I. The device demonstrated a strong performance with a short-circuit current density (*Jsc*) of 29.4 mA/cm^2, an OCV of 0.97 V, and an FF of 87.6%, resulting in an ultimately high PCE of 24.96%. The relatively steep slope of the J-V characteristics indicated a low series resistance, an efficient charge extraction, and low recombination losses in the solar cell architecture.

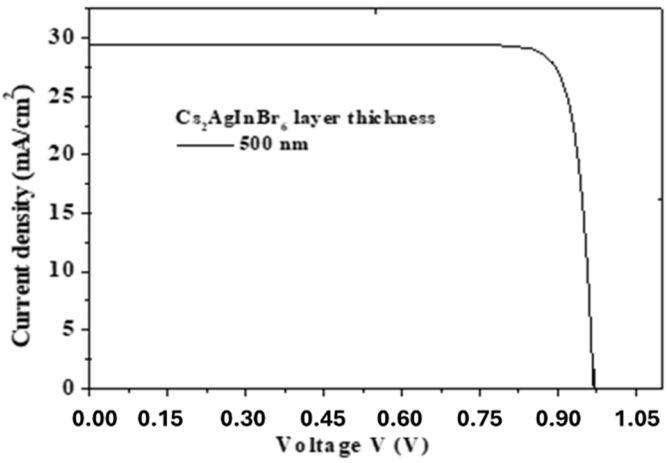

Fig. 3. Simulated J-V characteristics of the solar cell.

C. *Impact of Acceptor Density (N_A) in the $Cs_2AgInBr_6$ Active Layer*

The acceptor density (N_A) of the absorber layer is an important factor for solar cell optimization. To test this, N_A was varied from 1×10^{13} cm^{-3} to 1×10^{18} cm^{-3}, and its effect on the key photovoltaic parameters was analyzed (Figure 4).

In Figure 4(a), OCV remained stable up to $N_A = 1\times10^{15}$ cm^{-3}. For the acceptor density values above this value, the OCV increased monotonically to a maximum value of 1.186 V at the highest doping level (1×10^{18} cm^{-3}). On the other hand, *Jsc* was stable up to $N_A = 1\times10^{15}$ cm^{-3} and decreased sharply from $N_A = 1\times10^{15}$ cm^{-3} to $N_A = 1\times10^{16}$ cm^{-3} after which it was stabilized. In Figure 4(b), PCE followed the same trend with *Jsc*, while FF followed a similar trend to *Jsc* and PCE up to $N_A = 1\times10^{16}$ cm^{-3}. However, it exhibited a gradual recovery after this point.

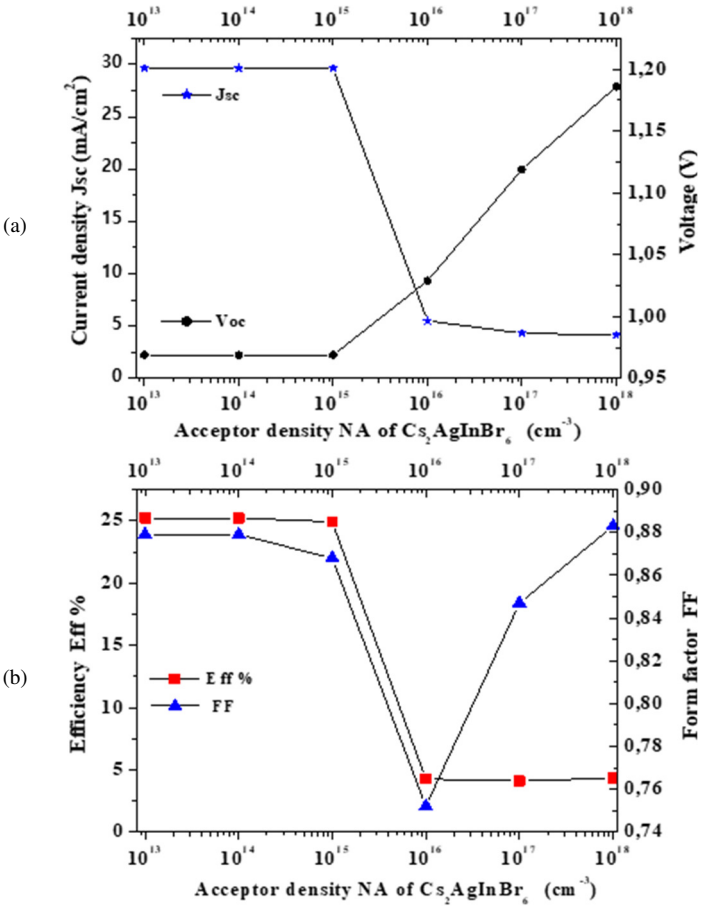

Fig. 4. The impact of acceptor density of doule perovskite ($Cs_2AgInBr_6$) layer.

These behaviors can be credited to the carrier dynamics under doping conditions. Acceptor doping increased the hole concentration (majority carriers), while it reduced the electron density (minority carriers), thereby enhancing the device's charge transport capacity. At intermediate doping levels, the balance between these effects optimized the device performance. At high doping levels ($N_A > 10^{16}$ cm^{-3}), *Jsc* and PCE were stabilized due to competing carrier dynamics. The increased hole concentration (majority carriers) enhanced the conductivity, and also elevated the Shockley-Read-Hall (SRH) recombination due to defect-assisted trapping [4, 10]. Additionally, the narrowing depletion region reduced the available volume for electron-hole pair generation. These losses are balanced by two mechanisms: (1) the band-tailing effects, where impurity bands merge with the valence band,

mitigating further losses in carrier mobility [17], and (2) the Fermi-level pinning near the valence band edge, which limits further increases in OCV, but stabilizes the charge extraction [16]. The results arose from simulation under ideal conditions, assuming uniform material properties, fixed 300 K operation, and simplified defect distributions. These assumptions may not fully capture real world complexities, like interface recombination or thermal effects [4, 10]. The predicted efficiency (24.96%) aligns with that of theoretical studies [15, 17] while exceeding current experimental reports for similar lead-free perovskites [4], highlighting the need for an experimental validation of the optimized parameters (500 nm thickness, $N_A = 10^{13}$-10^{15} cm^{-3}). Future work should incorporate defect engineering and temperature-dependent studies to bridge this simulation-experiment gap.

IV. CONCLUSION

This study optimized the performance of a $Cs_2AgInBr_6$ heterojunction solar cell using AMPS-1D simulations. Two key parameters were evaluated: absorber thickness and acceptor density. The results revealed that an optimal active layer thickness of 500 nm, combined with an acceptor density in the range of 10^{13}-10^{15} cm^{-3}, could maximize the device performance. Under these conditions, the solar cell achieved a remarkable PCE of 24.96%, with J_{SC} = 29.40 mA/cm^2, V_{OC} = 0.969 V, and FF = 87.6%. These findings provided actionable design guidelines for fabricating efficient, lead-free PSCs.

However, the simulations were conducted under idealized conditions, so there are some limitations. Therefore, it is important to validate the theoretical results through experimental studies. Future work should focus on the incorporation of theoretical predictions and experimental performance to ensure the device optimization.

REFERENCES

[1] Y. Liang, "Exploring inorganic and nontoxic double perovskites Cs2AgInBr6(1−x)Cl6x from material selection to device design in material genome approach," *Journal of Alloys and Compounds*, vol. 862, May 2021, Art. no. 158575, https://doi.org/10.1016/j.jallcom.2020.158575.

[2] Z. Zhang *et al.*, "Potential Applications of Halide Double Perovskite Cs2AgInX6 (X = Cl, Br) in Flexible Optoelectronics: Unusual Effects of Uniaxial Strains," *The Journal of Physical Chemistry Letters*, vol. 10, no. 5, pp. 1120–1125, Feb. 2019, https://doi.org/10.1021/acs.jpclett.9b00134.

[3] A. Menedjhi, N. Bouarissa, S. Saib, and K. Bouamama, "Halide double perovskite Cs2AgInBr6 for photovoltaic's applications: Optical properties and stability," *Optik*, vol. 243, Oct. 2021, Art. no. 167198, https://doi.org/10.1016/j.ijleo.2021.167198.

[4] V. Deswal, S. Kaushik, R. Kundara, and S. Baghel, "Numerical simulation of highly efficient Cs2AgInBr6-based double perovskite solar cell using SCAPS 1-D," *Materials Science and Engineering: B*, vol. 299, Jan. 2024, Art. no. 117041, https://doi.org/10.1016/j.mseb.2023.117041.

[5] A. Kojima, K. Teshima, Y. Shirai, and T. Miyasaka, "Organometal Halide Perovskites as Visible-Light Sensitizers for Photovoltaic Cells," *Journal of the American Chemical Society*, vol. 131, no. 17, pp. 6050–6051, May 2009, https://doi.org/10.1021/ja809598r.

[6] R. F. Service, "Perovskite Solar Cells Keep On Surging," *Science*, vol. 344, no. 6183, pp. 458–458, May 2014, https://doi.org/10.1126/science.344.6183.458.

[7] K. T. Butler, J. M. Frost, and A. Walsh, "Band alignment of the hybrid halide perovskites CH 3 NH 3 PbCl 3 , CH 3 NH 3 PbBr 3 and CH 3 NH 3 PbI 3," *Materials Horizons*, vol. 2, no. 2, pp. 228–231, 2015, https://doi.org/10.1039/C4MH00174E.

[8] A. Walsh, "Principles of Chemical Bonding and Band Gap Engineering in Hybrid Organic–Inorganic Halide Perovskites," *The Journal of Physical Chemistry C*, vol. 119, no. 11, pp. 5755–5760, Feb. 2015, https://doi.org/10.1021/jp512420b.

[9] B. K. Bareth, M. N. Tripathi, and R. Maravi, "High photovoltaic performance of lead-free Cs2AgInCl6-xBrx perovskite solar cell using DFT and SCAPS-1D simulations," *Materials Today Communications*, vol. 39, June 2024, Art. no. 108618, https://doi.org/10.1016/j.mtcomm.2024.108618.

[10] Y. Liu, I. J. Cleveland, M. N. Tran, and E. S. Aydil, "Stability of the Halide Double Perovskite Cs2AgInBr6," *The Journal of Physical Chemistry Letters*, vol. 14, no. 12, pp. 3000–3006, Mar. 2023, https://doi.org/10.1021/acs.jpclett.3c00303.

[11] X.-G. Zhao *et al.*, "Cu–In Halide Perovskite Solar Absorbers," *Journal of the American Chemical Society*, vol. 139, no. 19, pp. 6718–6725, May 2017, https://doi.org/10.1021/jacs.7b02120.

[12] O. Diachenko *et al.*, "Structural and Optical Properties of CuO Thin Films Synthesized Using Spray Pyrolysis Method," *Coatings*, vol. 11, no. 11, Nov. 2021, Art. no. 1392, https://doi.org/10.3390/coatings11111392.

[13] M. Khalid Hossain *et al.*, "Combined DFT, SCAPS-1D, and wxAMPS frameworks for design optimization of efficient Cs 2 BiAgI 6 -based perovskite solar cells with different charge transport layers," *Royal Society of Chemistry (RSC) Advances*, vol. 12, Dec. 2022, Art. no. 35002, https://doi.org/10.1039/D2RA06734J.

[14] S. K. Vasheghani Farahani *et al.*, "Principles of Chemical Bonding and Band Gap Engineering in Hybrid Organic–Inorganic Halide Perovskites," *Physical Review B*, vol. 119, no. 11, pp. 5755–5760, Oct. 2014, https://doi.org/10.1021/jp512420b.

[15] H. Sabbah, Z. Abdel Baki, R. Mezher, and J. Arayro, "SCAPS-1D Modeling of Hydrogenated Lead-Free Cs2AgBiBr6 Double Perovskite Solar Cells with a Remarkable Efficiency of 26.3%," *Nanomaterials*, vol. 14, no. 1, 2024, Art. no. 48, https://doi.org/10.3390/nano14010048.

[16] J. P. C. Baena *et al.*, "Highly efficient planar perovskite solar cells through band alignment engineering," *Energy & Environmental Science*, vol. 8, no. 10, pp. 2928–2934, 2015, https://doi.org/10.1039/C5EE02608C.

[17] K. Wang, Y. He, M. Zhang, J. Shi, and W. Cai, "Promising Lead-Free Double-Perovskite Photovoltaic Materials Cs2MM′Br6 (M = Cu, Ag, and Au; M′ = Ga, In, Sb, and Bi) with an Ideal Band Gap and High Power Conversion Efficiency," *The Journal of Physical Chemistry C*, vol. 125, no. 38, pp. 21160–21168, Sept. 2021, https://doi.org/10.1021/acs.jpcc.1c05699.

[18] I. Chandran, T. D. Subash, and M. Batumalay, "Simulation and Optimization of ZnO/CuO/Cds Solar Cell Using SCAPS," *NanoWorld Journal*, vol. 9, no. S5, pp. S97–S100, 2023.

[19] N. Benaissa *et al.*, "Experimental and numerical simulation studies of CuO thin films based solar cells," *Engineering Research Express*, vol. 5, no. 4, Nov. 2023, Art. no. 045038, https://doi.org/10.1088/2631-8695/ad05b3.

[20] P. Sawicka-Chudy *et al.*, "Simulation of TiO2/CuO solar cells with SCAPS-1D software," *Materials Research Express*, vol. 6, no. 8, June 2019, Art. no. 085918, https://doi.org/10.1088/2053-1591/ab22aa.

[21] M. Ichimura and Y. Kato, "Fabrication of TiO2/Cu2O heterojunction solar cells by electrophoretic deposition and electrodeposition," *Materials Science in Semiconductor Processing*, vol. 16, no. 6, pp. 1538–1541, Dec. 2013, https://doi.org/10.1016/j.mssp.2013.05.004.